# Mechanical Response of the Cervical Spine under Compression Loading

C. W. Roberts[1] J. Tocyzski[1], J. Moors[1], and J. R. Kerrigan[1]
[1] The University of Virginia; [2] Center for Applied Biomechanics

## ABSTRACT

*The objective of this study was to use whole body tests determine how torso mass is recruited during an inverted drop test, identify injuries caused at a impact velocity of 4.4 m/s, and to better understand vertebral kinematics during axial compression of the cervical spine. Five post-mortem human surrogates (PMHS) were suspended upside-down in a standard seating position, and were then dropped. The subjects were dropped on a padded five-axis load plate in order to determine the force experienced following initial contact. Subjects were dropped with a combination of impact velocities at levels of 2 m/s and 4.4 m/s. Each PMHS was instrumented with three blocks mounted along the thoracic spine and two blocks on the head. Every block contained three mutually orthogonal accelerometers and angular rate sensors. High-speed X-ray videos were captured to visualize the kinematics of the vertebrae. The force from the load cell followed the same characteristic double peak shape as seen in other studies. Typically, the first peak is assumed to be associated with the mass of the head acting on the load cell and the second peak is thought to be the effect of the torso mass. However, acceleration timing of the T1, T4 and T8 blocks suggest that part of the torso mass acts on load cell within the first peak of the loading. Most injuries from an inverted impact occurred between in the region of the lower cervical spine and the upper thoracic spine due to flexion of the cervical spine following initial impact. Kinematics data suggest the curvature of the spine before and during loading have a large influence on the likelihood and type of injury.*

## INTRODUCTION

Given the frequency and severity of cervical spine injuries resulting from rollover crashes, it is critical to analyze the mechanism of cervical spine injury in this loading condition. In a roof-to-ground impact, the vertical excursion of the occupant can exceed the available headroom, causing a head impact into the roof. The head contacting a deforming roof can act as a pocketing end condition for the head, restricting the head's motion while the torso compresses the neck (Burke et al., 2009). In order to better understand cervical spine injury in rollover crashes, it is necessary to study this compression loading through the head. Most of the research with this type of loading consists of component-level studies with a fixed T1 vertebra that have used a 16 kg mass as the effective mass of the torso (Nightingale, 1996, 1997 and Myers, 1991). In these tests, velocity of the mass has been the independent variable to determine at what threshold injury occurs. Clearly, this velocity criterion is heavily dependent on the effective mass of the body acting on the head and cervical spine. For example, if the assumed magnitude of the effective mass is too great, injury would occur at a much lower velocity. Few tests have analyzed the entire body during an inverted head impact; therefore, little is known regarding the effective mass of the torso and how mass is recruited following the impact.

Viano compiled injury data presented in biomechanical literature in which full body testing was performed for compressive spinal injury and only two studies have performed inverted drop testing (Viano 2008, Nusholtz 1983, Sances and Yoganandan, 1986). He specifically highlights the need for more data with impact velocity conditions between 2 and 4 m/s. A preliminary testing series consisting of four post mortem human surrogates (PMHS) subjected to inverted drop was performed at the Center of Applied Biomechanics at a velocity condition of 3.2 m/s, which has been suggested to be around the threshold of injury in component testing, and many injuries were found in component testing at this velocity level (Myers 1991, Nightingale 1996, Nightingale 1997). However, in this preliminary study with full body drops, no injuries from impact were found in all four of the PMHS tested (Foster 2013). Given this lack of injury with an impact condition of 3.2 m/s, this testing series presented here focused on testing subjects well below the threshold of injury, at 2 m/s, and above the 3.2 m/s velocity because it was found to be insufficient to cause injury in the preliminary testing series. The goals of this test series were to better understand the kinematics associated with the cervical and thoracic spine during impact, to analyze acceleration timing of thoracic vertebrae to provide insight on mass recruitment of the torso, and to perform injury analysis caused by a 4.4 m/s velocity condition.

## METHODS

Five male post-mortem human surrogates (PMHS) were selected for this sturdy based on an absence of pre-existing fractures, lesions or other cervical and thoracic spine bone pathology confirmed by computed tomography (CT) scans. The PMHS were obtained and treated in accordance with the ethical guidelines established by the Human Usage Review Panel of the National Highway and Traffic Safety Adminstration, and all the handling procedure were reviewed and approved by the Center for Applied Biomechanics Biological Protocol Committee and an independent Oversight Committee at the University of Virginia. The gender, age, height weight and bone density of the selected subjects is listed in Table 1, below.

Table 1: Specifications of each subject tested.

| **Subject Number** | **Gender** | **Age (years)** | **Height (mm)** | **Weight (kg)** | **Bone Density** |
|---|---|---|---|---|---|
| 582 | M | 71 | 1780 | 68.04 | 0.8 |
| 534 | M | 71 | 1715 | 93.16 | 0.8 |
| 606 | M | 62 | 1803 | 51.71 | -0.3 |
| 610 | M | 48 | 1721 | 61.69 | -2.6 |
| 693 | M | 47 | 1780 | 64.49 | -1.3 |

## Testing Configuration

During testing, each PMHS was suspended in an inverted standard seating position and dropped onto a foam padded six-axis load cell (Manary, 1998). This load cell measured the interaction between the impact surface and the skull, and it was padded to prevent skull fracture, as the goal of this study was to understand cervical spine injury. Each subject was placed in a military harness and then suspended using a network of strings and carabineers. Adjustable nylon strings were secured around the ankles, knees, thighs, pelvis, back and shoulders. The general test setup can be seen in Figure 1, which includes both a lateral and posterior view. This network of strings converged to a single carabiner, which was connected to a solenoid release mechanism. The release mechanism was attached to a gantry, which had height adjustment capabilities. Different impact velocity conditions were achieved by dropping the subject from different heights. Coarse height adjustment was accomplished with the ratchet system built into the gantry and fine adjustment was attained by using the chain hoist that attached the release mechanism and the gantry. Subjects 534 and 606 were tested multiple times, first at lower velocity conditions (considered non-injurious) and then at a higher velocity level. Subjects 582, 610 and 693 were each tested only once at higher velocity levels. An extra chain hoist with lots of slack was attached to each subject just before testing. This chain hoist was used as an arresting strap, to prevent the body weight from rolling onto the neck following the test, which might cause an injury not associated with the impact. The X-Ray setup consisted of an X-Ray source, two image intensifiers and a high speed camera. The X-Ray source was positioned 254 cm away from the face of the image intensifier. The X-Ray source was directed towards the left side of each subject's head, while the image intensifier was on the right side of the subject's head, as close to the subject as possible without interfering with the subject's motion during the drop test.

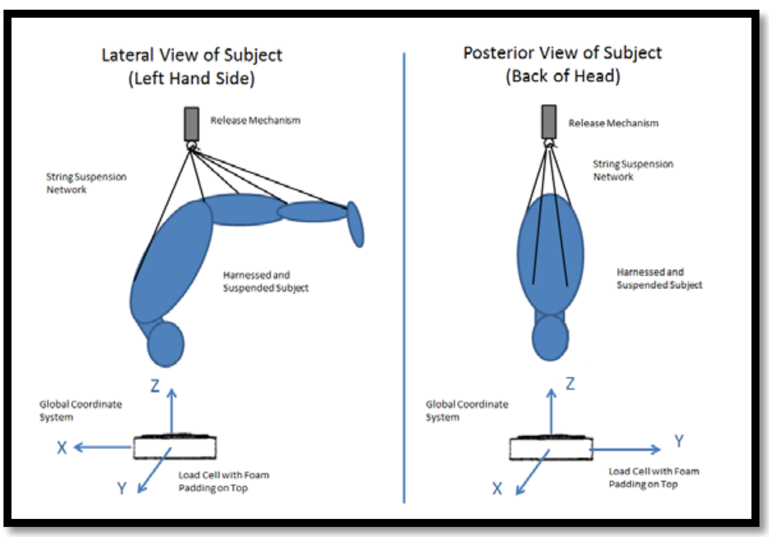


Figure 1: A schematic of the test setup including both lateral and posterior views of the suspended subject

## PMHS Preparation and Instrumentation

Before any preparations began, each PMHS was weighed and the standard NHTSA anthropometry measurements were recorded. Then, the arms of each subject were removed at the sternoclavicular joint. In previous testing series, it was found that high-speed X-ray video images were heavily distorted by the arms; the arms were removed in the hopes of getting clearer X-ray images during the impact. Three screws were placed in the skull that denoted the location of the plane in which the center of gravity of the head lies. The plane was found by marking a straight line between the inferior lateral corner of the orbital margin of one of the eyes and the tragus of the ear on the same side of the head. These marks were repeated for the other side of the head as well. A screw was placed at a vertical location one third of the distance between the marked line and the apex of the head and a horizontal position 8.5 mm anterior to the tragus. A third screw was placed in the back of the head, halfway between the left and right screws and parallel to the lines marked on the face. Also, two mounting plates were screwed into the left and right sides of the skull. Six degree of freedom blocks consisting of three linear accelerometers and three angular rate sensors were affixed to both of these mounting plates.

Next, a transverse cut was made slightly lateral to the middle of back in order to ensure no damage was done to the anterior longitudinal ligament (ALL) or any of the other tissue or musculature that might compromise the dynamic response of the spine. Static X-rays, like the one pictured in figure 2, geometric calculations, and previous CT scan images were using to place 2 long pedicle screws through the each of the T1, T4 and T8 vertebral bodies. In Figure 2, there are two pedicle screws placed in the T1 vertebra and one pedicle screw in the T4 vertebral body. The other thin pins are spinal needles which helped denote the location of each vertebra, but were removed before testing. After all of the pedicle screws were in place, the transverse cut was sewn up with the pedicle screws above skin level. Mounts were clamped around the two pins associated with T1, T4 and T8. Six degree of freedom blocks were affixed to each of these mounts to record kinematics of the vertebrae. Finally, all orifices and cuts were sewn up and sealed with RTV in order to prevent leakage, and each subject was wrapped in a thin layer of mechanically adhesive wrap.

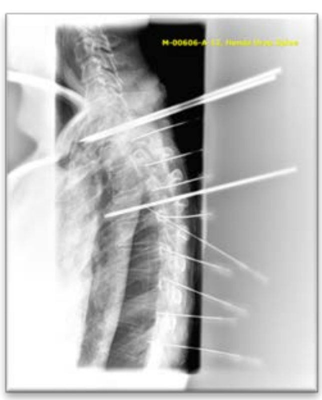

Figure 2: A static X-ray image of subject 582 during instrumentation of the thoracic spine.

## Positioning and Testing

After preparing each PMHS, a CT scan was taken to check that the pins traveled through the T1, T4 and T8 vertebral bodies, ensure that no unintentional damage had occurred during preparation, and to determine the relative position of the T1 vertebral body to its associated mounting plate outside of the body. Knowing this relationship was crucial to positioning each suspended subject, as the goal was to position the T1 vertebral body 25 degrees from horizontal to match the position in the Nightingale and Myers tests ( ). Also, the CG plane, marked by the screws placed in the skull during preparation was positioned such that it was 0 degrees from the horizontal, completely parallel to the floor. X-ray was captured for all of the tests with the exception of tests 6 and 7. The solenoid release mechanism malfunctioned the day of those tests, thus a manual release had to be used. The high-speed X-Ray video could not be taken while someone was in the testing area for radiation safety purposes. Also, immediately following test 9, the subject was injured following the first drop because the arresting strap was too short.

## Kinematic Analysis

The first step in the kinematic analysis was to determine which coordinate systems could be used to easily describe the motion. Accelerometer and angular rate data were recorded in the coordinate system in which the accelerometers and angular rate sensors are mounted; this means each mount, each block, and each accelerometer needs to be rotated and translated in order to move the recorded linear accelerations and angular rates to a global coordinate system and to the local coordinate system associated with each vertebra. The definition for all of the vertebral coordinate systems is the same and is determined by the geometry of each individual vertebra.

X, Y and Z coordinates for all four corners of each mounting plate were taken from the CT scans, as well as coordinates for the left lateral process (L), the right lateral process (R) and the most posterior point of the spinous process (P) of T1, T4 and T8. These points are illustrated in Figure 9, the superior view of the T1 vertebra. The coordinate system of each of the vertebrae was defined using the same process. First, the y-axis was defined by the vector of the point L, the left lateral process to the point R, the right lateral process. Next, the origin point, O, was defined as the intersection of the y-axis and its perpendicular line that includes point P, the most posterior point of the spinous process. Thus, the positive y-axis was defined as the vector from point P to point O. The positive z-axis was found by taking the cross product of the positive x-axis and the positive y-axis. The lateral view of the vertebral system is seen in the Figure 3. The lateral view of the vertebral system in Figure 3 shows both the positive x and z-axes, and figure 9, the superior view of the vertebra, shows the positive x and y-axes. Although Figure 3 shows the T1 vertebra, the coordinate systems for T4 and T8 are defined in the using the same landmarks and the same method. The accelerometer and angular rate blocks on the head were moved to the CG of the head using the FARO points on each face of the left and right cubes and the position of the screws on the left, right and posterior of the head. The y-axis was found by finding the vector of the location of the left screw, L and to the location of the right screw, R. Next the x-axis of the head was found by finding the perpendicular line to the y-axis on which point P, the posterior of the head, lies. The intersection of the x- and y-axis is the location of the origin, which is also the center of gravity (CG) of the head. The positive x-axis was found my taking the cross product of the positive x-axis and the positive y-axis.

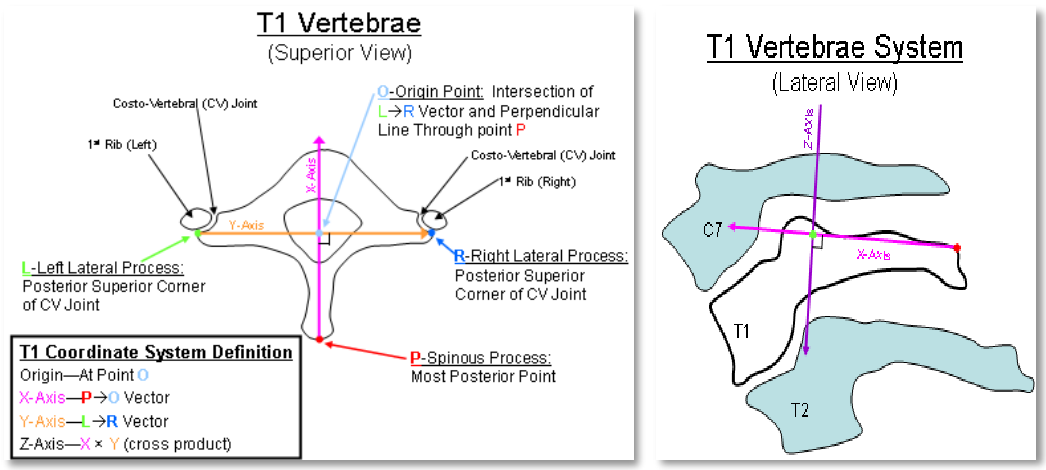


Figure **3**: A diagram of the superior and lateral view of the vertebral coordinate system for T1.

After preparation of each PMHS, a FARO arm was used to determine the exact position of the screws in the head that define the plane in which the head CG lies as well as the position of all three faces of the blocks on the left and right sides of the head. Then, just prior to dropping each subject, after the final position had been determined, the x, y and z faces of the T1, T4 and T8 blocks were scanned using a ROMER arm. The screws on the head were scanned with the ROMER arm as well. Having the locations and orientations of all of these points and planes allowed for the formation of rotation matrices

After the rotation matrices were found, the accelerometer data and angular rate data were used to form accelerations of the in the vertebral coordinate system using Equations 1, 2 and 3, below. In these equations, $a_{0z}$, $a_{0y}$, and $a_{0z}$ are the transformed accelerations in the vertebral coordinate system, $a_{pz}$, $a_{py}$, and $a_{pz}$ are the accelerations in the accelerometer coordinate system (raw data), $\omega_x$, $\omega_y$, and $\omega_z$, are angular velocities and $\alpha_x$, $\alpha_y$, and $\alpha_z$, are angular accelerations.

$$a_{0x} = a_{px} - \omega_x(\omega_y r_y + \omega_z r_z) + r_x(\omega_{y2} + \omega_{z2}) - \alpha_y r_z + \alpha_z r_y \qquad \textbf{\textit{Equation 1}}$$
$$a_{0y} = a_{py} - \omega_y(\omega_x r_x + \omega_z r_z) + r_y(\omega_{x2} + \omega_{z2}) - \alpha_z r_x + \alpha_z r_z \qquad \textbf{\textit{Equation 2}}$$
$$a_{0z} = a_{pz} - \omega_z(\omega_x r_x + \omega_y r_y) + r_z(\omega_{x2} + \omega_{y2}) - \alpha_x r_y + \alpha_y r_x \qquad \textbf{\textit{Equation 3}}$$

The above equations yielded the accelerations in the x, y, and z directions of the local coordinate systems of the CG of the head, T1, T4 and T8. These accelerations were later used to determine kinematics of the motion of each of the individual vertebrae as well as the motion of the head. Later, these accelerations were translated to the global coordinate system using the top plate of the load cell onto which each subject was dropped as a reference. This global data allowed for the determination of the exact position of the body before drop as well as giving global acceleration, velocity and position data for the right and left sides of the head and the T1, T4 and T8 vertebrae.

## RESULTS

Following testing, each subject was taken for a third and final CT scan, and after that scan, an autopsy was performed. Combined information from the CT scans and autopsies helped to determine injury in each PMHS. The impact velocities were determined following the testing by determining the time between the drop and initial impact and assuming the subject was falling only vertically in a uniform gravity field. The impact velocity conditions calculated for each test can be found in Table 2, below.

Table 2: Calculated impact velocities for each test.

| Test Number | Subject Number | Impact Velocity (m/s) |
|---|---|---|
| 6 | 582 | 4.27 |
| 7 | 534 | 2.00 |
| 8 | 534 | 4.35 |
| 9 | 606 | 2.03 |
| 10 | 606 | 2.00 |
| 11 | 606 | 4.45 |
| 12 | 610 | 4.41 |
| 13 | 693 | 4.43 |

### Injuries

All five of the PMHS had injuries in the thoracic or cervical spine following testing. Most of the injuries occurred at the lower level of the cervical spine and at higher levels of the thoracic spine. The injuries for each subject can be seen in Table 3, below. Most of these injuries seem to be caused by flexion and extension loading. Figure 4 shows a CT scan of subject 606 and specifically points out the fractures on the superior endplate of T1 and the inferior endplate of C7.

Table 3: List of injuries for each subject post-testing.

| Subject | Injury description |
|---|---|
| 582 | • Fracture of anterior arch of C1<br>• Fracture at T3 superior/T4 inferior fact joint<br>• Body fracture of T4 that extends through screw hole<br>• Fracture at T4 superior/T5 inferior facet joint<br>• All ligaments and facet capsules intact |
| 534 | • Subtle non-displaced fracture along the anterior and lateral walls of right maxillary sinus as well as a mild fragmentation of nasal spine<br>• Two transverse fractures of C3 vertebral body<br>• Acute coronal oblique fracture in the T2 vertebral body<br>• Flexion injury to the intervertebral joint at T1/T2<br>• Supraspinous ligament and interspinous ligament rupture, and a |

| | |
|---|---|
| | partial rupture of the ligamentum flavum at level of T1/T2<br>• Extended fractures between T1 and T5 |
| 606 | • Acute fracture of superior endplate of T1<br>• Acute fracture of inferior endplate of C7<br>• Tear in anterior longitudinal ligament at C6/C7 level<br>• Major disruption of C7/T1 joint including ruptured facet joints and ruptured interspinous and supraspinous ligament |
| 610 | • Rupture of anterior longitudinal ligament at C3/C4<br>• Acute non-displaced fracture on superior endplate of T1 that was not associated with the pedicle screws<br>• Acute fracture inferior endplate of C7<br>• Major disruption of C7/T1 joint including ruptured facet joints, and ruptured interspinuous and supraspinous ligaments and the ligamentum flavum |
| 693 | • Major disruption of T1/T2 joint including ruptured left facet joint, complete rupture of interspinous ligament and the supraspinous ligament, and a partial rupture of the posterior longitudinal ligament<br>• Left facet joint of C7/T1 very loose |

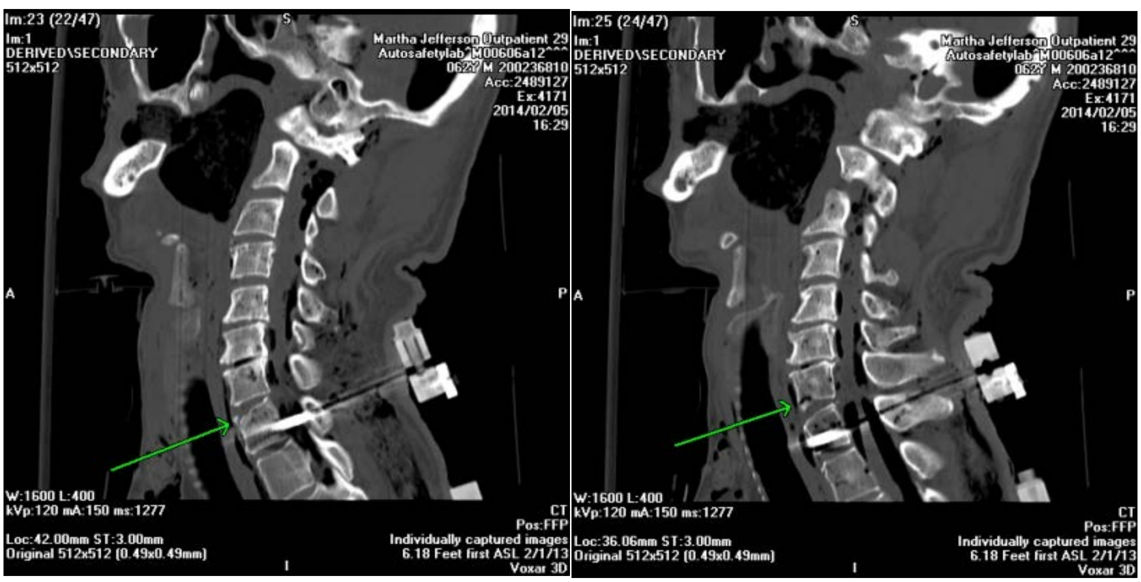


Figure **4**: A fracture of C7 (left) and a fracture of T1 (right) for Subject 606.

**Kinematics**

The maximum force recorded by the load cell normal to the impact surface was recorded for each test. This maximum force from each impact is recorded in Table 3, below, with respect to its calculated velocity condition. There is a clear difference in the range of the impact force for the tests around 2 m/s and the tests around 4.4 m/s.

Table 3: The maximum force corresponding to the velocity of each test.

| Test Number | Subject Number | Impact Velocity (m/s) | Maximum Force (N) |
|---|---|---|---|
| 6 | 582 | 4.27 | 7718.988 |
| 7 | 534 | 2.00 | 2171.779 |
| 8 | 534 | 4.35 | 7761.851 |
| 9 | 606 | 2.03 | 2453.654 |
| 10 | 606 | 2.00 | 2213.837 |
| 11 | 606 | 4.45 | 11674.096 |
| 12 | 610 | 4.41 | 9978.372 |
| 13 | 693 | 4.43 | 11361.796 |

These impact forces are plotted against the impact velocity in Figure 5, below. Included in Figure 5 are data from inverted drop testing performed by Nusholtz, Yoganandan and Sances.

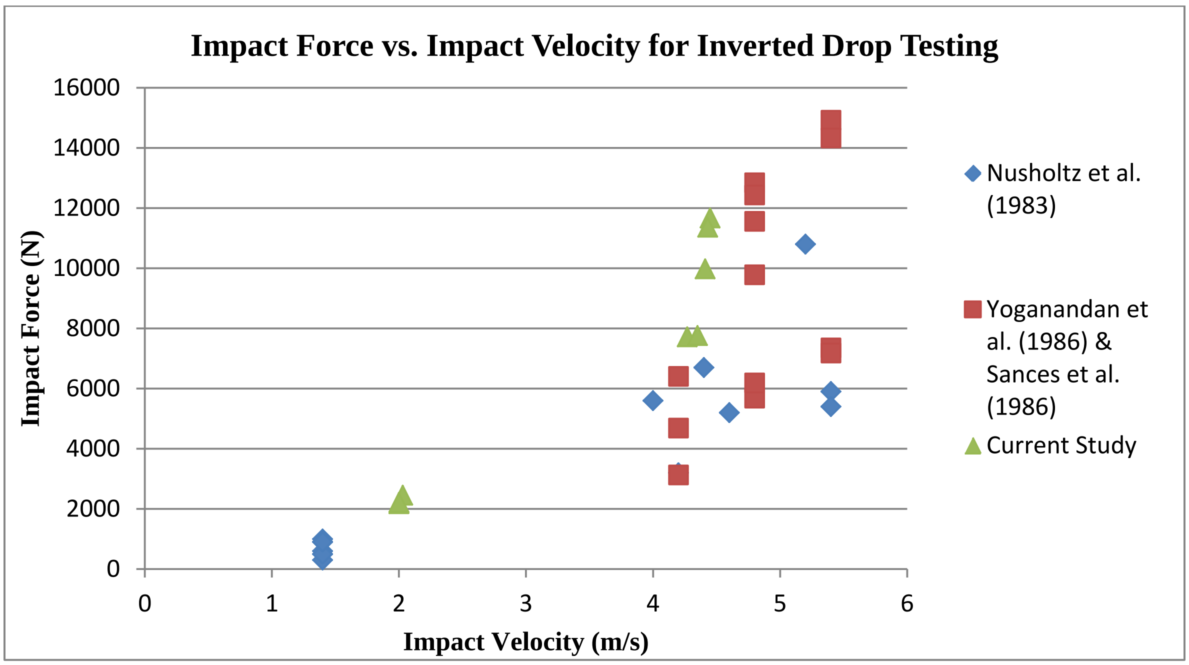


Figure 5: A comparison of the forces and velocities in inverted drop testing in the literature.

Using the local acceleration data in the T1, T4 and T8 coordinate systems and the local acceleration data at the CG of the head, it was possible to determine the timing as to when the skull and T1, T4 and T8 vertebral bodies began to experience force from the impact. These times were determined as the first time when the resultant acceleration time trace for each exceeded the noise threshold in the data. These times were determined for the accelerometers on the left and right of the head, and the T1, T4 and T8 accelerometers and can be found in Table 4.

Table 4: A table of the times at which the resultant accelerations pass the noise threshold.

| Test Number | Subject Number | Impact Velocity (m/s) | Head L Start Time (ms) | Head R Start Time (ms) | T1 Start Time (ms) | T4 Start Time (ms) | T8 Start Time (ms) |
|---|---|---|---|---|---|---|---|
| 6 | 582 | 4.27 | 1.03 | 0.847 | 3.27 | 2.37 | 2.05 |
| 7 | 534 | 2.00 | 1.93 | 1.99 | 3.98 | 3.14 | 3.98 |
| 8 | 534 | 4.35 | 2.26 | 1.07 | 3.13 | 2.82 | 2.76 |
| 9 | 606 | 2.03 | 0.487 | 0.296 | 6.40 | 5.27 | 5.20 |
| 10 | 606 | 2.00 | 1.56 | 2.14 | 6.90 | 5.75 | 5.63 |
| 11 | 606 | 4.45 | 1.80 | 1.58 | 1.92 | 1.73 | 1.67 |
| 12 | 610 | 4.41 | 0.040 | 0.129 | 1.72 | 1.28 | 1.38 |
| 13 | 693 | 4.43 | 0.279 | 0.256 | 0.033 | 2.44 | 2.40 |

As seen in Table 4, the sensors on the left and right sides of the head experience an increase in acceleration at almost the same time for all of the tests. It should be noted that in most tests, an increase in acceleration in T4 or T8 occurs before an increase in acceleration in T1. The timings for three of the tests, Test 6, Test 11, and Test 12, can be seen in a graphical format in Figures 6, 7, and 8. The red trace is the impact force versus time, and the colored lines represent when each part of the body begins to accelerate.

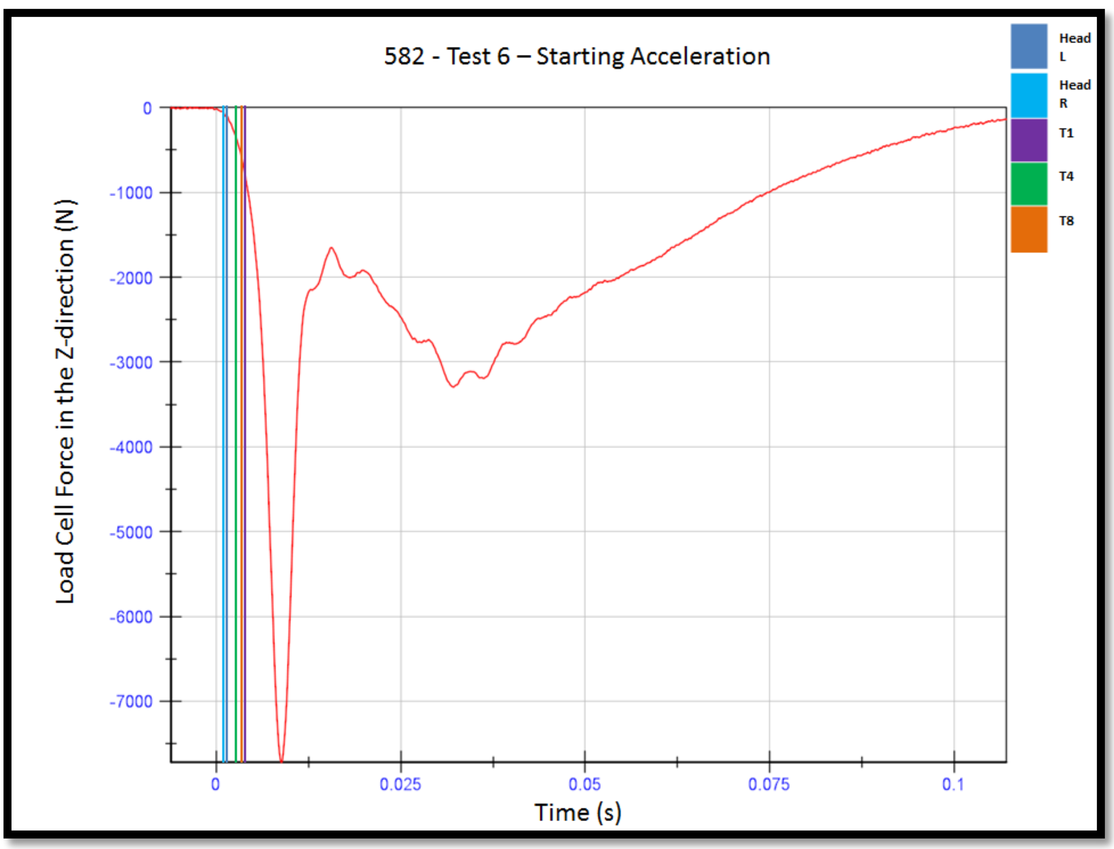


Figure 6: A plot of the starting accelerations and force trace for Test 6.

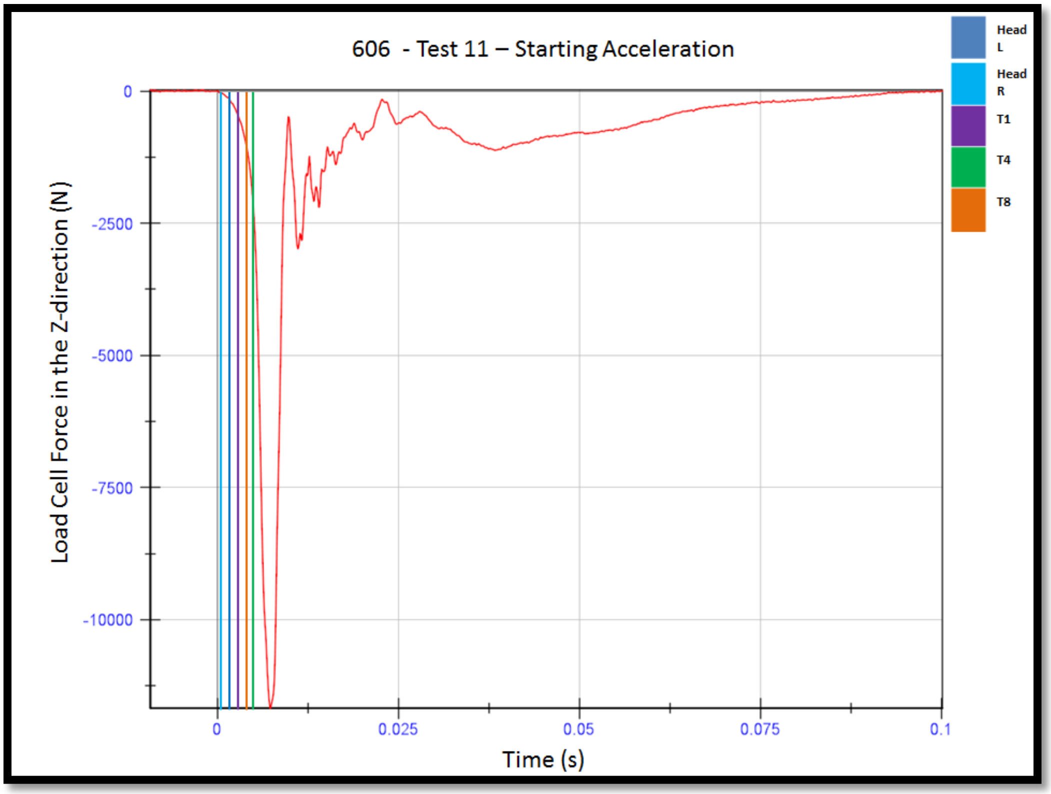


Figure 7: A plot of the starting accelerations and force trace for Test 11.

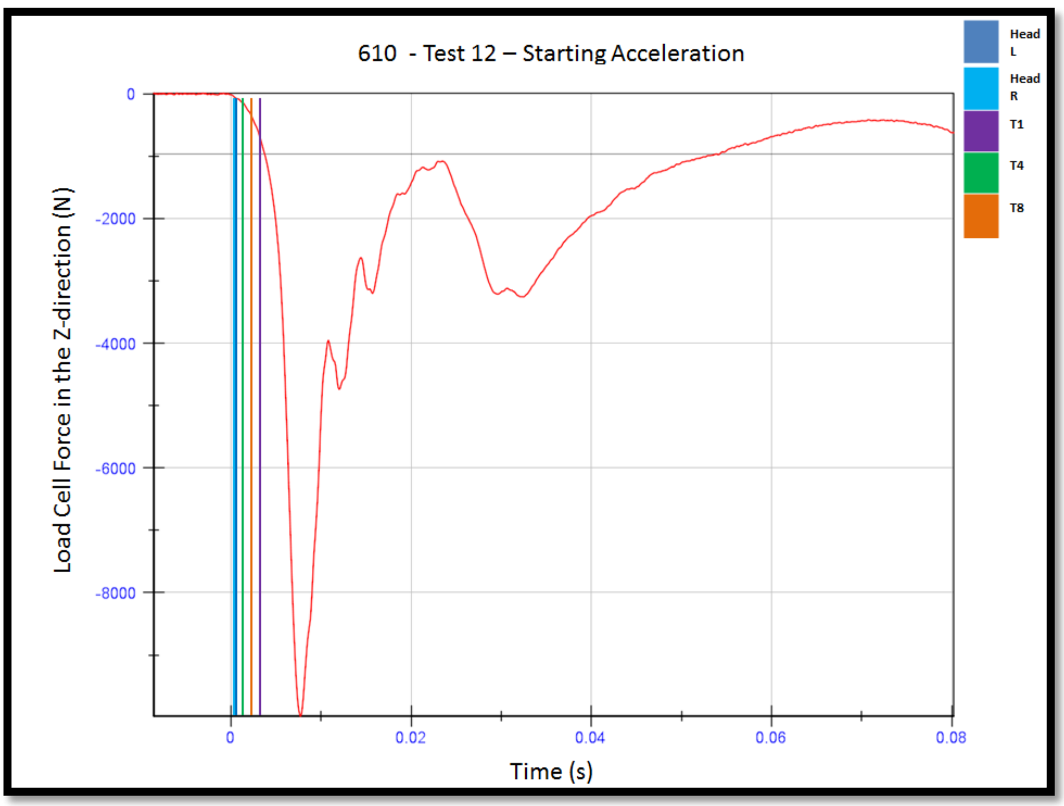


Figure 8: A plot of the starting accelerations and force trace for Test 12

The time at which the peak resultant acceleration occurred in the left head, right head, T1, T4, and T8 sensor blocks was also determined from the local acceleration data. Similar to the starting time data, in most of the tests the peak in the acceleration for T4 or T8 came before the peak acceleration for T1. The timing of the peak accelerations for three of the tests, Test 6, Test 11, and Test 12, are shown in Figures 9, 10 and 11. The time scale in these figures is slightly different than that of Figured 6, 7, and 8; it focuses on the first peak with larger magnitude of the characteristically shaped double peak force response for compression loading of the neck.

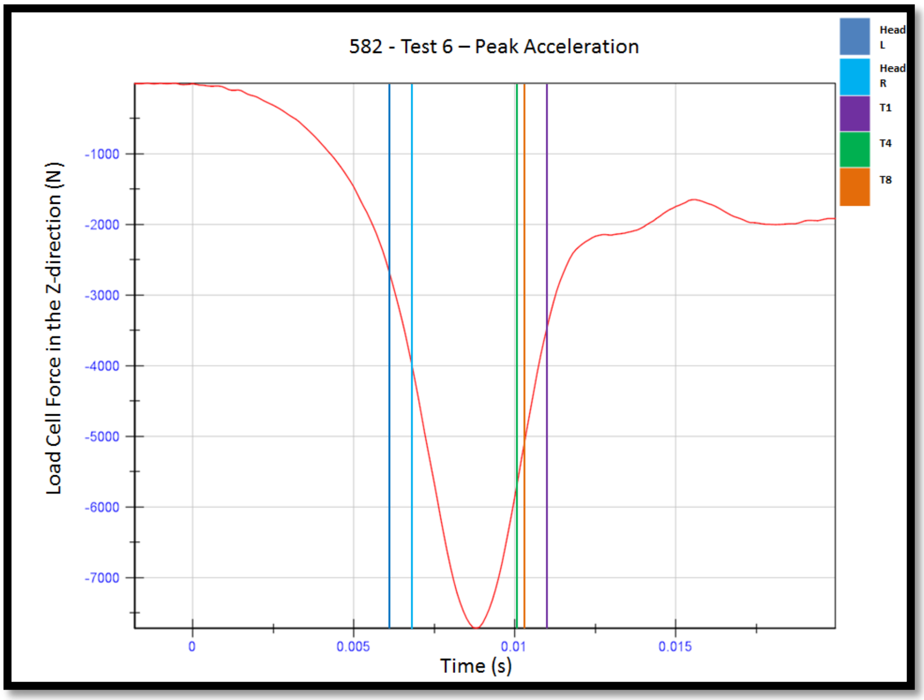

Figure 9: A plot of the time of peak accelerations and force trace for Test 6.

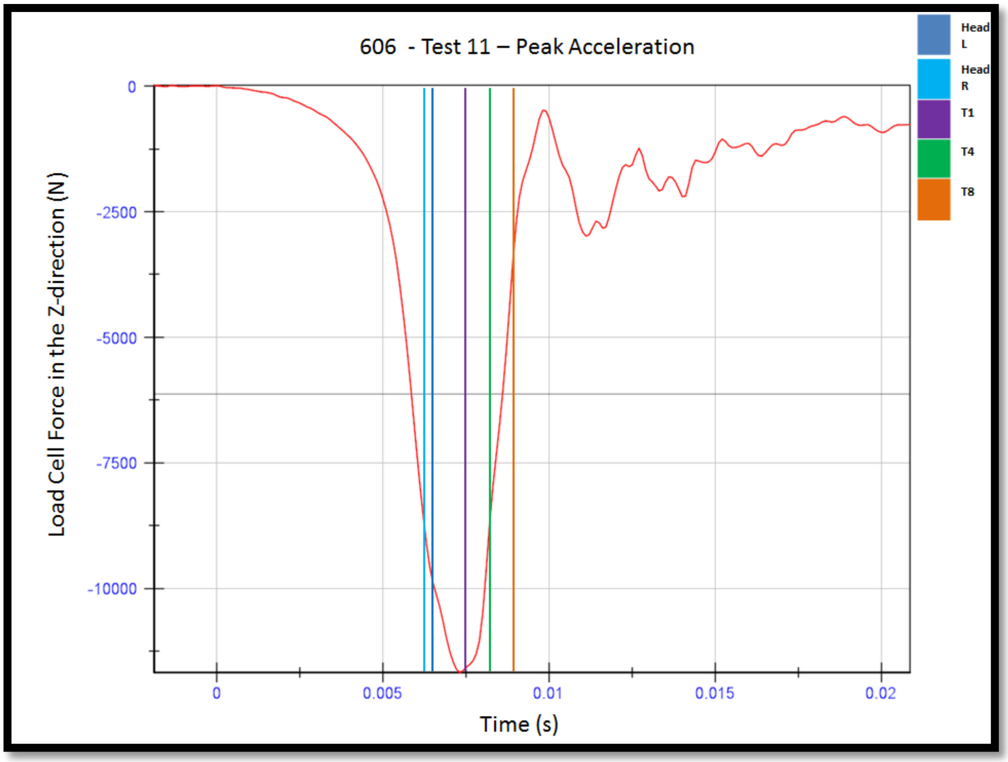


Figure 10: A plot of the time of peak accelerations and force trace for Test 11.

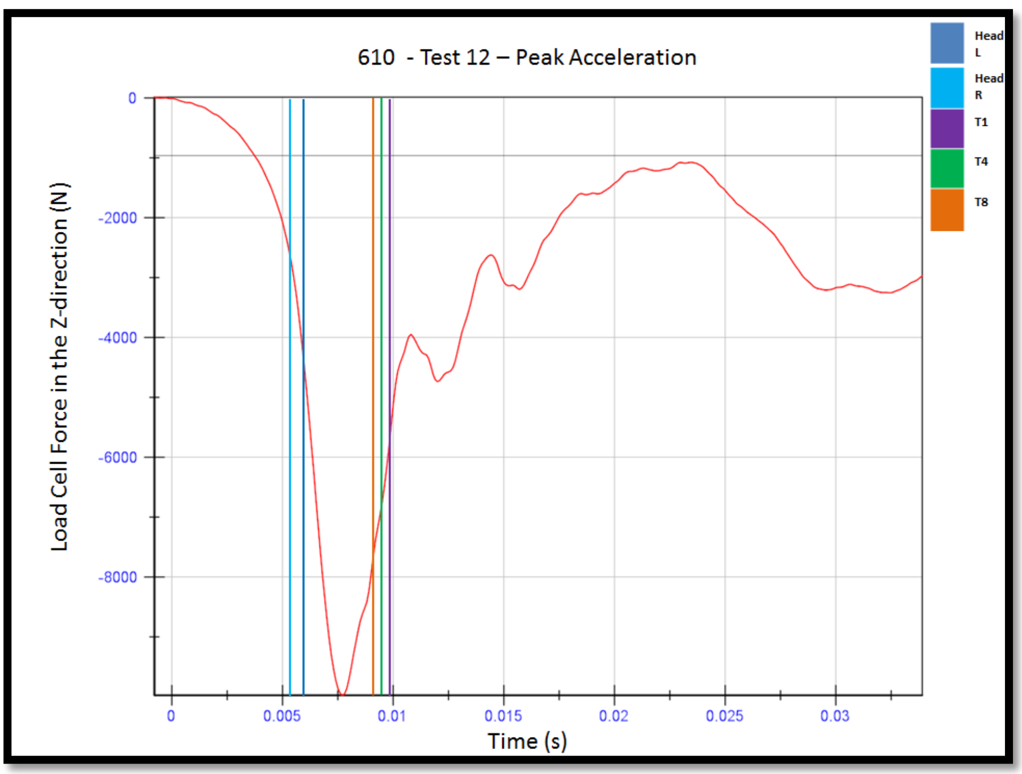


Figure 11: A plot of the time of peak accelerations and force trace for Test 12.

## Imaging

Although high speed X-ray videos were taken during most of the tests, determining accurate kinematics from the images proved difficult. Although removing the arms from each subject significantly reduced the amount of tissue through which the X-rays had to pass, each subject had varying amounts of tissue and bone, meaning different X-ray settings had to be determined and then used for each subject. Further image processing and analysis will be performed to determine more kinematic information from these tests.

# DISCUSSION

Although the test data from the current study yielded higher maximum impact forces at tests with velocity conditions around 4 m/s, the data from this test still fits within the rest of the dataset seen in Figure 5. The difference in force magnitude between tests with an impact velocity around 4 m/s could result from difference in testing methods, including differences in impact location, presence or lack of padding on impact surface, presence of skull fractures, and if the position of the head and neck were either restrained or free.

The double peak shaped force response found in this study has been published in the findings by several authors studying neck compression (Nusholtz et al., 1981, 1983; Nightingale et al., 1997; Pintar et al., 1990). In previous studies, a simple rigid body lumped-parameter model where the mass of the head and the mass of the torso are connected by a spring is typically used to explain this biphasic force response; often the first peak in force is assumed to be due to the acceleration of the head mass and the second peak is assumed to be due to the acceleration of a portion of the mass of the torso. The timing of starting accelerations seen in Table 4 and Figures 6,7, and 8 suggest that the head, T1, T4, and T8 begin to experience accelerations before the maximum impact force is reached. Also, the timing of the peak accelerations for the head, T1, T4, and T8 occur during or just following the first peak of the force. This timing data suggests that the first mass in the rigid body lumped- parameter model is not just the mass of the head, but rather the mass of the head coupled with the torso up to at least the level of T8 or that this two mass model is not an accurate representation of the true kinematics of the system.

Comparing to injuries in the literature for inverted drop testing, many of the same injuries found in this study were achieved by Nusholtz, Yoganandan and Sances (1983, 1986, 1986). Also, it is interesting to note that many of the subjects tested at impact velocities around 4 m/s had injuries at the level of the lower cervical spine and the upper thoracic spine (C6-C7 and T1-T2). The type of fractures as well as the injury location suggests that flexion of the thoracic spine is the mode of injury for most of the injuries at this impact velocity. It is likely that these injuries occur after the initial peak force of the force trace had been achieved. Many of the injuries to the upper cervical spine occur at very high velocities. It is possible that these higher impact velocities have enough energy to cause injury upon initial impact, during the first peak of the biphasic force trace.

## CONCLUSIONS

Given the timing information and injury patterns with different velocities, the curvature of the thoracic and cervical spine seem to play a crucial role in the way force is transmitted throughout the spine following an inverted impact. More research is required to better understand the effects this curvature of the spine has on injury; if the head is impacted at different locations at the same velocity the loading of the spine could change drastically, causing different injuries and mechanisms of injury.

The effective mass causing the first peak in the force trace recorded by the load cell encompasses more than just the mass of the head. Data from this study show that the effective mass includes at least the mass between the skull and T8.

## REFERENCES


BURKE, D. S., BIDEZ M. W., MERGL K. (2009). Cervical spine tolerance to catastrophic injury in rollover crash environments. Proceedings from ASME. 591-2.

FOSTER, J. B. (2013). Injury Mechanisms and Priorites for Cervical Spine Trauma Mititgation in Rollover Crashes: The development and analysis of in vitro testing of axial compressive cervical spine impacts. Master thesis, University of Virginia.

MANARY, M. A., REED M. P., FLANNAGAN C. A., SCHNEIDER L. W. (1998). ATD Positioning Based on Driver Posture and Position. 42nd Stapp Car Crash Conference. 1-13.

MYERS B. S., NIGHTINGALE R. W., MCELHANEY J. H., DOHERTY D. J., RICHARDSON W. J. (1991). The Influence of end condition on human cervical spine injury mechanisms. Society of Automotive Engineers. 391-99.

NIGHTINGALE, R. W., MCELHANEY, J. H., CAMACHO, D. L., KLEINBERGER, M., WINKELSTEIN, B. A., & MYERS, B. S. (1997). *The dynamic responses of the cervical spine: buckling, end conditions, and tolerance in compressive impacts*(No. 973344). SAE Technical Paper.

NIGHTINGALE, R. W., MCELHANEY, J. H., RICHARDSON, W. J., & MYERS, B. S. (1996). Dynamic responses of the head and cervical spine to axial impact loading. *Journal of biomechanics*, *29*(3), 307-318.

NUSHOLTZ G. S., MELVIN J. W., HUELKE D. F., ALEN N. M., BLANK J. G. (1981). Response of the cervical spine to superior-inferior head impact. Proc of the 25th Stapp Car Crash Conf. 197-237.

NUSHOLTZ, G. S., HUELKE, D., LUX, P., ALEM, N. M., & MONTALVO, F. (1983). Cervical spine injury mechanisms. In *Proceedings of the International Research Council on the Biomechanics of Injury Conference* (Vol. 1983, pp. 179-198). International Research Council on Biomechanics of Injury.

PINTAR F. A., SANCES A., YOGANANDAN N. (1990). Biodynamics of the total human cervical spine. Proc of the 34th Stapp Car Crash Conf. 55-72.

VIANO, D. C., & PARENTEAU, C. S. (2008). Analysis of head impacts causing neck compression injury. *Traffic injury prevention*, *9*(2), 144-152.

YOGANANDAN, N., SANCES A., MAIMAN, D. J., MYKLEBUST, J. B., PECH, P., & LARSON, S. J. (1986). Experimental spinal injuries with vertical impact. *Spine*, *11*(9), 855-860.